RSC Advances

PAPER

View Article Online
View Journal | View Issue

Cite this: *RSC Adv.*, 2019, **9**, 37870

Preparation and microwave absorption performance of a flexible Fe_3O_4/nanocarbon hybrid buckypaper and its application in composite materials†

Jia Wang, Jian Jiao,* Guangmei Sun, Kai Yuan, Ziyi Guan and Xinyi Wei

Graphene oxide (GO) and carbon nanotubes are promising microwave-absorbing materials. Herein, ferroferric oxide (Fe_3O_4)/multiwall carbon nanotube (MWCNT) and Fe_3O_4/GO hybrid buckypapers with excellent flexibility and manoeuvrability were coated on the surface of an epoxy substrate to fabricate microwave-absorbing composites. Fe_3O_4/GO buckypapers show a unique layered structure that differs from the complex network structure of Fe_3O_4/MWCNT buckypapers. Therefore, the Fe_3O_4/GO buckypapers exhibit lower tensile strength and toughness than the Fe_3O_4/MWCNT buckypapers, and the minimum electromagnetic reflection loss of Fe_3O_4/GO buckypapers is higher than that of Fe_3O_4/MWCNT buckypapers. Further, Fe_3O_4/GO buckypapers have a wider effective absorption-frequency band than Fe_3O_4/MWCNT buckypapers at 2.0–18.0 GHz. Although the mechanical properties of epoxy resin composites coated with Fe_3O_4/MWCNT or Fe_3O_4/GO buckypapers show a slight deterioration in comparison with those of the epoxy resin substrate, both buckypapers exhibit improved microwave-absorption performance compared with the epoxy resin substrate.

Received 14th September 2019
Accepted 11th November 2019

DOI: 10.1039/c9ra07406f

rsc.li/rsc-advances

1. Introduction

The rapid development of military detection technology in various countries has been accompanied by an increasing demand for high-performance absorbing materials. Through magnetic loss or dielectric loss, unwanted electromagnetic waves that are effectively absorbed by electromagnetic-wave-absorbing materials can be converted into other forms of energy.[1] Traditional absorbing composite materials are formed through the direct combination of magnetic loss materials—such as ferrite and carbonyl iron—with electric loss materials—such as conductive polymers, carbon nanotubes and graphene.[2–4] However, adding a small amount of nanoparticles significantly increases the viscosity of the matrix as the nanoparticles easily agglomerate, which is not only detrimental to practical operation but also affects the mechanical and absorption properties of composite materials.[5–7] Therefore, increasing the dosage of nanoparticles and evenly distributing them in the absorbing composite materials simultaneously is a key factor in determining their effectiveness in absorbing materials.[8,9]

Carbon nanosheets (carbon nanopapers or buckypapers), prepared from pure carbon materials or compound nanoparticles, have been widely used in supercapacitors, micromedia polarisation and flexible energy storage. In recent years, buckypapers gradually came into focus and were used as an ideal microwave-absorbing materials because of their lightness, excellent mechanical properties and high electrical conductivity.[10–13] The preparation methods for buckypapers can be classified into vacuum filtration assembly,[14] evaporation-induced self-assembly,[15] spin-coating,[16] drop-casting,[17] Langmuir–Blodgett (LB) methods,[18] spraying,[19] dip coating[20] and Langmuir–Schaefer methods. Common buckypapers include carbon nanotube,[21] graphene oxide (GO),[22–24] graphene[25,26] and carbon nano-fibre buckypapers.[27] Carbon nanotube buckypapers are made from randomly wound carbon nanotube sheets through vacuum filtration or other papermaking processes involving filtering a suspension through a thin mesh bracket. However, GO buckypapers, are self-supporting films comprising neatly arranged GO nanocrystals. GO buckypapers have a layered structure comprising individual, well-organised sheets 100–200 nm thick.[22] However, pure nanometre carbon buckypapers exhibit poor absorption performances owing to the large dielectric losses. Therefore, it is necessary to improve the impedance-matching performance of microwave-absorbing materials to prepare hybrid buckypapers by introducing magnetic materials.[7,28]

Department of Applied Chemistry, School of Science, Northwestern Polytechnical University, Xi'an, Shaanxi, 710072, P. R. China. E-mail: jjiao@nwpu.edu.cn

† Electronic supplementary information (ESI) available. See DOI: 10.1039/c9ra07406f

Lu *et al.*[8] prepared ferric oxide (Fe_3O_4)/multiwall carbon nanotube (MWCNT) sandwich buckypapers *via* layer deposition. The results showed that the electromagnetic reflection loss (RL) of the buckypaper could reach −12.62 dB at 17.72 GHz, making it a high-frequency-microwave-absorbing material with excellent application prospects. Ma *et al.*[29] prepared a rGO/F-NP hybrid film *via* an improved thermal reduction method. They studied the effects of adding carbon fibre micro-powders on the microwave absorption characteristics and mechanical properties of thin films. The results showed that when the nanoparticle content was 200 mg, the hybrid film had the best absorption performance, with a minimum RL of −22.18 dB at 10.64 GHz. However, to the best of our knowledge, minimal research has been reported on applying buckypapers as microwave-absorbing coatings on epoxy resin/fibre composites.

This paper demonstrates that combining the advantages of Fe_3O_4/MWCNT and Fe_3O_4/GO flexible hybrid buckypapers and epoxy resin/fibre composites is a promising method for preparing absorbing light and thin composite materials with wide absorption frequency bands and good absorption ability. Through detailed investigation, we found that introducing flexible buckypapers significantly improves the processing performance of the composites compared with that of the traditional Fe_3O_4/carbon material powder absorbent. More importantly, the prepared Fe_3O_4/MWCNT and Fe_3O_4/GO flexible hybrid buckypapers/epoxy resin/fibre composites exhibit excellent microwave-absorption performances, which is helpful in realising applications of buckypapers as absorbing agents and absorbing materials.

2. Experimental

2.1 Materials

MWCNT (OD: 10–20 nm, length: 10–30 μm, purity: >98 wt%) were purchased from Zhongke Era Nano. Fe_3O_4 nanoparticles (200 nm, 99.5%) were provided by Shanghai Macklin Biochemical Co., Ltd., China. γ-Aminopropyltriethoxysilane (APTES) was obtained from Nanjing Crompton Shuguang Organosilicon Specialities Co., Ltd., China. 1-(3-Dimethylaminopropyl)-3-ethyl carbodiimide hydrochloride (EDC) was obtained from Macklin Biochemical Co., Ltd., China. *N*-Hydroxysuccinimide (NHS) was purchased from Shanghai Aladdin Biochemical Co., Ltd., China. Amine-terminated polyoxyethylene ether (D230, flexible epoxy curing agent) was purchased from Guangdong Huntsman Advanced Chemical Materials Co., Ltd., China.

2.2 Preparation of Fe_3O_4/MWCNT hybrid buckypapers

The Fe_3O_4/MWCNT buckypapers were prepared according to ref. 8. A calculated volume of suspension (150, 300 or 450 ml) was poured into a vacuum filtration device through a 0.45 μm water-based cellulose filter paper to obtain buckypapers with different thicknesses (0.04, 0.08 or 0.12 mm). The buckypapers were labelled C_1, C_2 and C_3 (corresponding to different Fe^{3+} contents) and C_4, C_5 and C_6 (corresponding to different thicknesses of C_2 buckypapers).

2.3 Preparation of Fe_3O_4/GO hybrid buckypapers

The GO aqueous solution was prepared according to ref. 30. Fe_3O_4 nanoparticles (0.4 g) were added to the ethanol/water (1 : 1, volume ratio) mixed solution, and ultrasonication was performed for 30 min until the mixture was evenly dispersed. Then, the mixed solution was transferred to a 250 ml three-necked flask, and APTES was added dropwise ($n_{Fe_3O_4} : n_{KH\text{-}550} = 1 : 4$) under a nitrogen atmosphere. The mixture was reacted at 85 °C for 2 h and subsequently aged at the same temperature for 30 min. The brown precipitate was poured into a beaker and washed several times with deionised water and anhydrous ethanol. Finally, modified Fe_3O_4 nanoparticles were obtained after vacuum drying at 60 °C overnight.

A certain amount of GO aqueous solution was dispersed in deionised water and ultra-sonicated for 30 min; then, 150 ml of the mixed solution was poured onto a self-made PMMA plate mould and placed in a vacuum oven at 60 °C overnight to obtain single-layer GO buckypaper. Similarly, 300 ml of the mixed solution was added in two equal amounts according to the aforementioned steps to obtain double-layer GO buckypaper. EDC and NHS (the mass ratio of GO : EDC : NHS was 10 : 5 : 4) were added to evenly dispersed GO aqueous solution, and continuously stirred for 30 min. Then, modified Fe_3O_4 nanoparticles (the mass ratios of GO : Fe_3O_4 were 1 : 1, 8 : 2, 7 : 3 and 6 : 4) were added to aforementioned mixture and further stirred for 30 min. The mixture obtained from this process (150 ml) was poured on the self-made PMMA plate mould and placed overnight in a vacuum oven at 60 °C to obtain single-layer Fe_3O_4/GO buckypapers with varying Fe_3O_4 contents. Similarly, 300 ml of the mixture was added in two equal amounts according to the aforementioned steps to obtain double-layer Fe_3O_4/GO buckypaper. The single and double-layer Fe_3O_4/GO buckypapers were labelled S_1, S_2, S_3, S_4, S_5 and S_6, S_7, S_8, S_9, S_{10}, respectively, corresponding to Fe_3O_4 contents of 0, 20, 30, 40 and 50 wt%, respectively. The preparation mechanism and reaction scheme for Fe_3O_4/GO buckypapers are shown in Fig. 1 and 2.

2.4 Preparation of composites

E-51 epoxy resin and curing agent D230 were mixed in a mass ratio of 100 : 35 and uniformly coated on the surfaces of the C_2 and S_4 buckypapers prepared as described in Section 2.2. The flexible buckypapers were obtained when the resin was completely cured at room temperature. Fe_3O_4/MWCNT and Fe_3O_4/GO flexible buckypapers were spread on the surface layer after the fibre cloth was laid up according to the manufacturing method for the hand lay-up FRP (mass ratio of E-51 epoxy resin to D230 curing agent was 100 : 35). Finally, the composite materials were placed in a thermos-compressor under the pressing conditions 60 °C/1 h + 80 °C/2 h + 100 °C/1 h + 120 °C/1 h, and the Fe_3O_4/MWCNT buckypapers/EP/GF and Fe_3O_4/GO buckypapers/EP/CF composites were obtained through cooling in the furnace.

2.5 Characterisation

Fourier transform infrared (FT-IR) spectra of the buckypapers were obtained by using a IS10 instrument (Nicolet, USA) in the

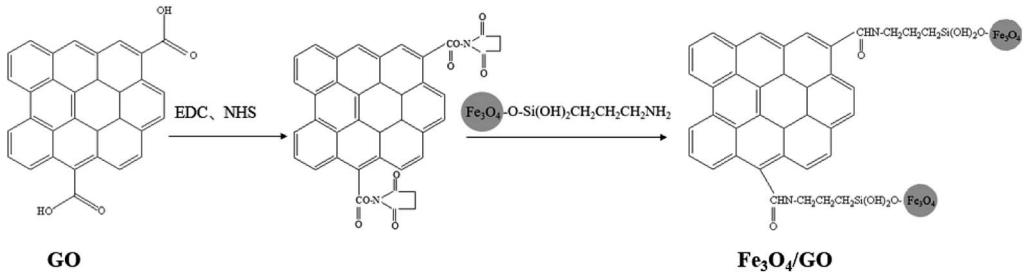

Fig. 1 Preparation mechanism of Fe_3O_4 nanoparticles loaded with GO.

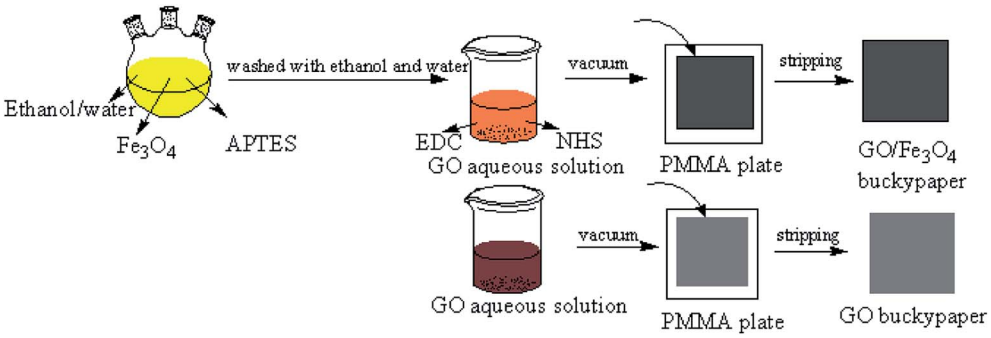

Fig. 2 Reaction scheme for GO and Fe_3O_4/GO buckypapers.

range 4000–400 cm^{-1}. X-ray photoelectron spectroscopy (XPS) was performed using a Kratos Axis Ultra DLD spectrometer with a monochromatic Al Kα X-ray source. The morphologies of the buckypapers and composites were characterised through scanning electron microscopy (SEM, Quanta 600FEG, FEI, USA). The lamellar structure of GO was characterised by transmission electron microscopy (TEM, FEI, USA). The tensile strengths of the buckypapers were measured using an Edberg tensiometer. The mechanical properties of the composites were determined at ambient temperatures according to the GB/T 1449-2005, GB/T 1450.1-2005 and GB/T 1447-2005 method using a UTM5000 united testing system (Xinsansi, Shenzhen). The electromagnetic RL values of the buckypapers and composites were characterised by a Hitachi Anritsu MS4644A vector network analyser using the waveguide method in the range of 2.0–18.0 GHz.

3. Results and discussion

3.1 Structure and properties of buckypapers

The FT-IR spectra of Fe_3O_4/MWCNT and Fe_3O_4/GO buckypapers with various iron contents are shown in Fig. 3a and b. The bands at 3433, 1631 and 1350 cm^{-1} in Fig. 3a correspond to the O–H stretching mode of water, C–C stretching vibration and the

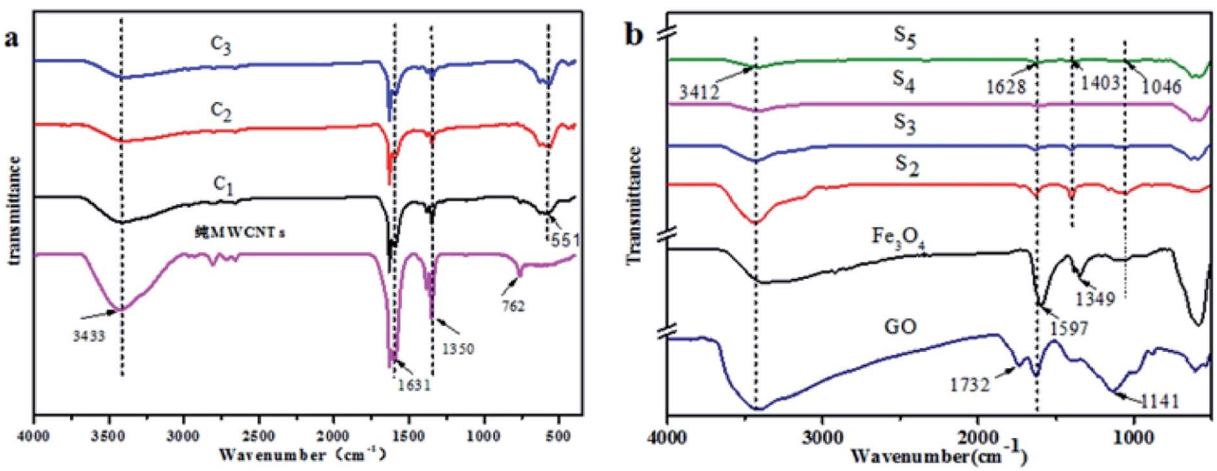

Fig. 3 FT-IR spectra of Fe_3O_4/MWCNT buckypapers (a) with different $m_{Fe_3O_4}$ to m_{MWCNT} ratios: (C_1) 1 : 1, (C_2) 2 : 1 and (C_3) 3 : 1 and Fe_3O_4/GO buckypapers (b) with different $m_{Fe_3O_4}$ to m_{GO} ratios: (S_2) 2 : 8, (S_3) 3 : 7, (S_4) 4 : 6 and (S_5) 5 : 5.

C–H stretching vibration of the MWCNT, respectively. Moreover, an additional band at 551 cm^{-1} can be ascribed to the lattice absorption of Fe_3O_4, further confirming the successful preparation of Fe_3O_4 NPs. In Fig. 3b, the infrared bands of GO indicate the presence of various oxygen-containing functional groups, including bands at 3412 cm^{-1} (O–H stretching vibration of water), 1732 cm^{-1} (C=O stretching of carboxyl groups at the edges of the GO networks) and 1628 cm^{-1} (O–H bending vibration of carboxyl), while the band at 1141 cm^{-1} could be due to the C–O stretching of the carboxyl groups. However, the spectrum of Fe_3O_4/GO buckypapers differs from that of GO under the influence of electrostatic forces. Two new characteristic bands at 1628 cm^{-1} (CO–NH stretching vibration) and 1403 cm^{-1} (C–N stretching of amide) demonstrate the successful covalent bonding between Fe_3O_4 and GO.

Fig. 4a and b shows a wide scan spectrum of Fe_3O_4/MWCNT buckypapers and the Fe 2p spectrum. The sharp peaks observed in the wide scan spectrum confirm the presence of C 1s, O 1s and Fe 2p. In the Fig. 4b, the peaks at 711.29 and 724.48 eV originate from Fe $2p_{3/2}$ and Fe $2p_{1/2}$ of Fe, corresponding to Fe^{2+} and Fe^{3+} in Fe_3O_4, respectively; however, there are no peaks at 710.35 and 724.0 eV representing Fe_2O_3. Fig. 4c shows the wide scan spectra of GO and Fe_3O_4/GO buckypapers. The peak observed in the wide scan spectrum of Fe_3O_4/GO confirms the presence of C 1s, O 1s, N 1s and Fe 2p. The C 1s spectra of GO buckypapers are shown in Fig. 4d, and these comprise three components: C=C (282.5 eV) in the aromatic rings, C–O (284.7 eV) of epoxy and alkoxy and C=O (286.5 eV) groups. On introducing Fe_3O_4, the C–N bond (285.2 eV) appears in the C 1s spectrum of Fe_3O_4/GO buckypapers and the other three parts shift to a higher binding energy, as shown in Fig. 4e, indicating the successful loading of modified Fe_3O_4 nanoparticles.

The optical photos and SEM images of tensile fracture sections of C_2 and S_4 buckypapers are shown in Fig. 5. Fig. 5a shows the smooth surface of C_2 buckypaper, which is free-standing and black. An optical image of S_4 buckypaper prepared *via* evaporation-induced self-assembly is shown in Fig. 5d. Compared with Fe_3O_4/MWCNT buckypaper, the Fe_3O_4/GO buckypaper is a self-supporting thin film comprising aligned GO nanosheets, and its surface is rough and uneven. This is probably because the vacuum filtration process makes the Fe_3O_4/MWCNT buckypaper compact. The photos of bent C_2 and S_4 buckypapers in Fig. 5b and e, respectively, show that they have good flexibility and the latter bends much more easily. Fig. 5c shows a section of C_2 buckypaper, the cross-section appears flat and the hybrid nanoparticles are uniformly distributed. The section of buckypaper in Fig. 5f shows the well-stacked structure of GO and presence of Fe_3O_4 nanoparticles in the buckypaper, unlike the cross-section of Fe_3O_4/MWCNT buckypaper.

As shown in Fig. 6, the morphologies of Fe_3O_4/MWCNT buckypapers with different Fe_3O_4 contents were demonstrated through SEM. Fig. 6a–d show that the MWCNT are entangled owing to van der Waals interactions. Fig. 6b shows Fe_3O_4 magnetic nanoparticles that are uniformly attached to the MWCNT surfaces with no detectable aggregation grew around the original particles as their content increased, and more MWCNT were coated with Fe_3O_4 nanoparticles. Fig. 6d shows a slight agglomeration of nanoparticles, which could be caused by their surface effects.

The structures and morphologies of single-layer GO and Fe_3O_4/GO buckypapers were characterised by SEM and TEM as shown in Fig. 7. Fig. 7a shows the folded structure of GO, which is beneficial to nanoparticle adhesion. Go has a clear layered

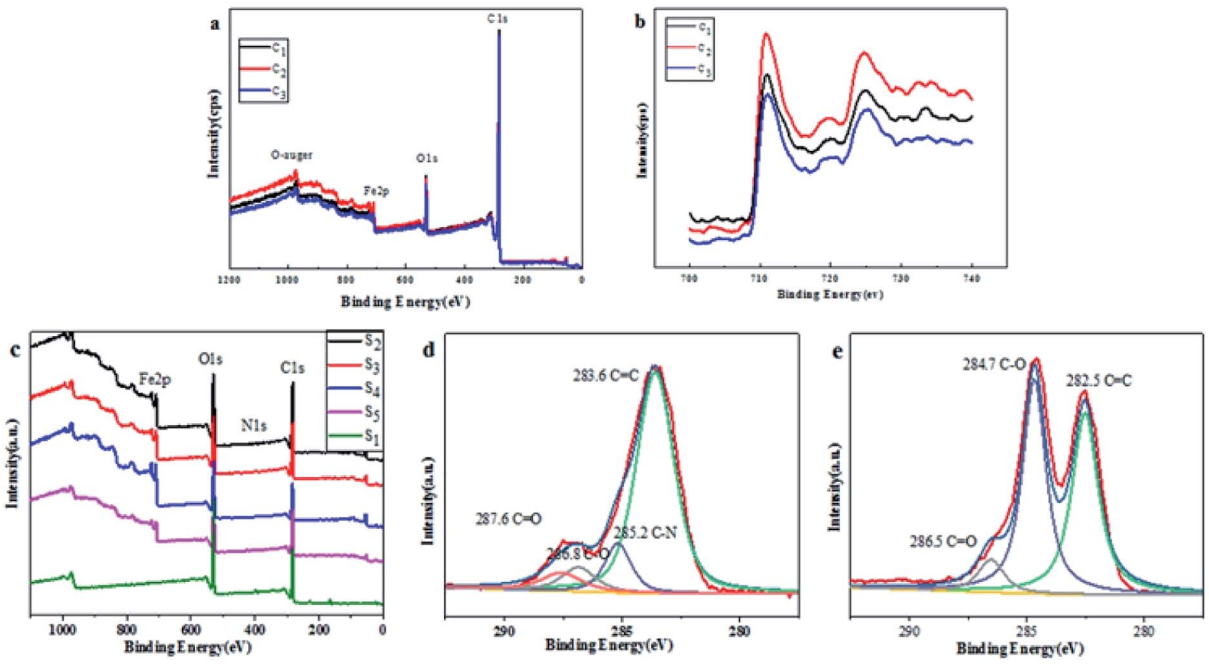

Fig. 4 XPS spectra: wide scan of Fe_3O_4/MWCNT (a) and Fe 2p spectrum of Fe_3O_4/MWCNT (b); wide scan of Fe_3O_4/GO buckypapers (c); C 1s spectra of GO (d) and Fe_3O_4/GO (e) buckypapers.

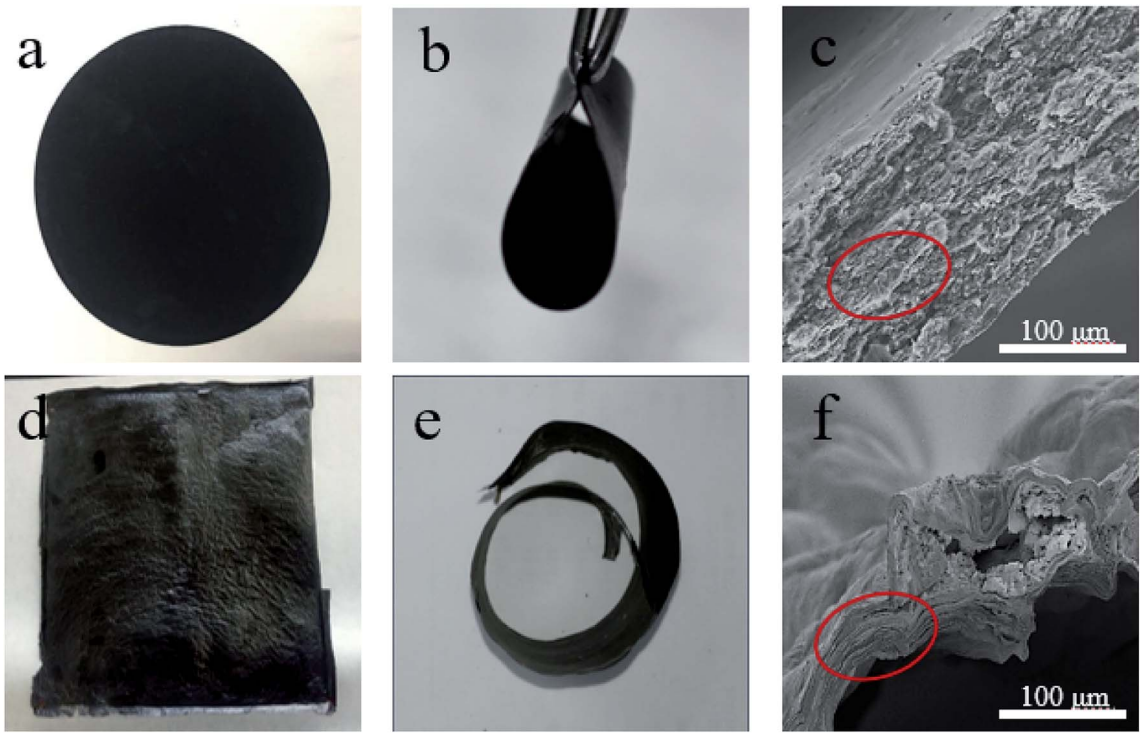

Fig. 5 Optical photos of straight and bent forms and SEM images of tensile fracture section of C_2 buckypaper (a–c) and S_4 buckypaper ($m_{Fe_3O_4}$: $m_{GO} = 6 : 4$) (d–f).

structure, and Fig. 7b shows that it is a transparent film, indicating its successful preparation. As shown in Fig. 7c–f, the Fe_3O_4/GO buckypapers have a 3D mesh structure and some nanoparticles are evenly distributed on the surface of the GO sheet, indicating excellent combination between the GO sheet and Fe_3O_4 nanoparticles. Additionally, a proportion of the nanoparticles were encapsulated inside the GO sheet, which partially prevented their agglomeration. The size of the nanoparticles increased with the Fe_3O_4 content in the buckypapers, which helped to enhance the interfacial contact between the GO layers and Fe_3O_4 nanoparticles.

To understand the relationship between the structure and mechanical properties of buckypapers, the tensile strengths of different types of buckypapers were tested using a tensiometer according to the GB/T940.3-2006 thin-film tensile-test method standard; the results are shown in Fig. 8. Fig. 8a shows the tensile strengths of Fe_3O_4/MWCNT buckypapers with different Fe_3O_4 contents, the results indicate that the tensile strength of the buckypapers increased approximately threefold when Fe_3O_4 nanoparticles were added, and this may be related to the denser structure of carbon nanotubes, which can be explained by the increased electrostatic forces between Fe_3O_4 and carbon nanotubes stabilising the particle-coating process. Fig. 8b shows that the thickness of the buckypapers minimally affects the tensile strength of the C_2 buckypapers, which may be because the unaltered structure of the buckypapers.

After adding nanoparticles, the tensile strength of Fe_3O_4/GO buckypapers was lower than that of pure GO buckypapers, as shown in Fig. 8c. The tensile strengths of single and double-layer S_2 and S_4 buckypapers were 1.14 and 0.98 MPa (S_2) and only 0.71 and 0.53 MPa (S_4), respectively. When the mass ratio of Fe_3O_4 to GO was 5 : 5, the tensile strength of the buckypapers increased slightly, which is probably related to the GO-sheet rearrangement. The presence of Fe_3O_4 nanoparticles affected the layered stacking structure of GO possibly because the Fe_3O_4 nanoparticles attached between graphene sheets weaken the forces between GO sheets during composite formation, and the stacking becomes slightly loose, decreasing the tensile strength of the Fe_3O_4/GO buckypapers, which is consistent with the SEM results. Conversely, carbon nanotubes are quasi-one-dimensional linear structures with a high length-to-diameter ratio. In buckypapers prepared using carbon nanotubes, these are wound around each other to form a complex network structure. Therefore, they have better mechanical properties than GO buckypapers.

The RL values of hybrid Fe_3O_4/MWCNT buckypapers with different Fe_3O_4 content, which vary with frequency from 2.0–18.0 GHz, are shown in Fig. 9a. The minimum RL from C_1 buckypaper can reach −13.4 dB at 16.2 GHz, and the RL bandwidth below −10 dB is 1.8 GHz (from 15.2 to 17.0 GHz). For the C_2 buckypaper, we observed a significantly improved absorption performance compared with the former. The minimum RL can reach −26.4 dB at 16.3 GHz, the RL bandwidth below −10 dB (>90% absorption) is 6.0 GHz (from 11.6 to 17.6 GHz), and RL values below −20 dB (>99% absorption) are achieved in the range 14.9–17.2 GHz. While C_3 buckypaper exhibits only week electromagnetic wave absorption, its minimum RL can reach −7.6 dB at 16.4 GHz. As the mass ratio

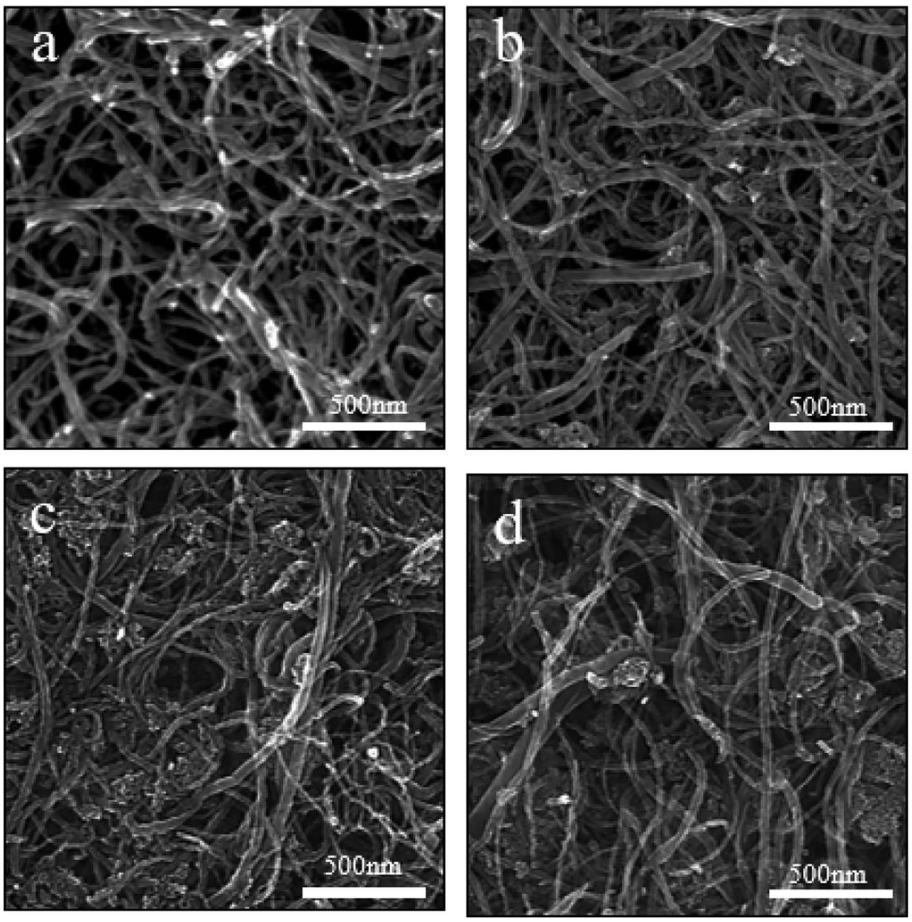

Fig. 6 SEM images of Fe_3O_4/MWCNT buckypapers with different $m_{Fe_3O_4}$ to m_{MWCNT} ratios: (a) 0 : 1, (b) 1 : 1, (c) 2 : 1 and (d) 3 : 1.

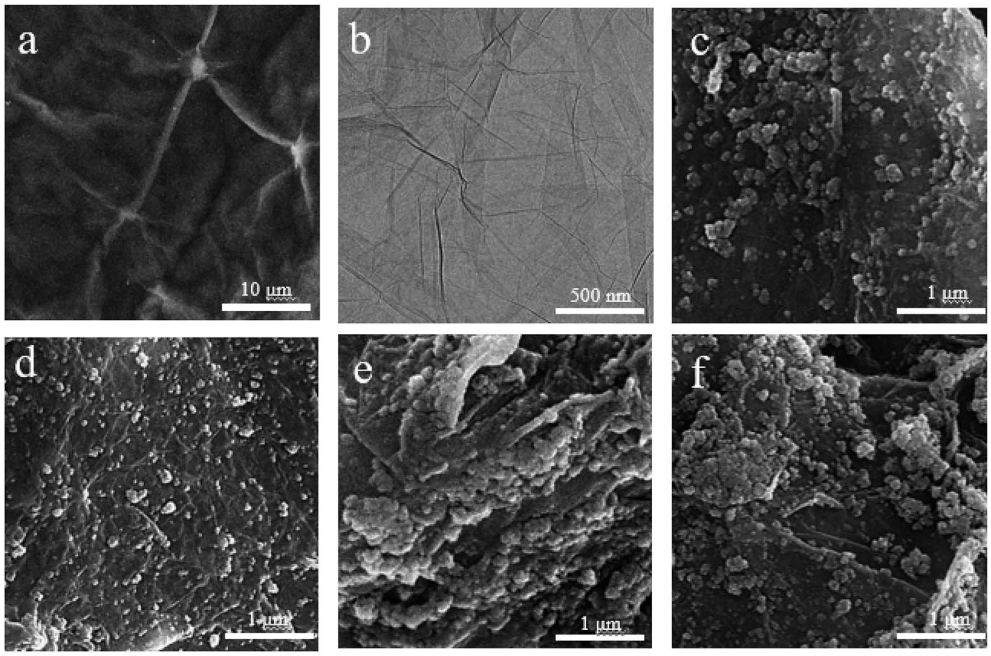

Fig. 7 TEM and SEM images of GO (a and b) and Fe_3O_4/GO buckypapers with different $m_{Fe_3O_4}$ to m_{GO} ratios: (c) 8 : 2, (d) 7 : 3, (e) 6 : 4 and (f) 5 : 5.

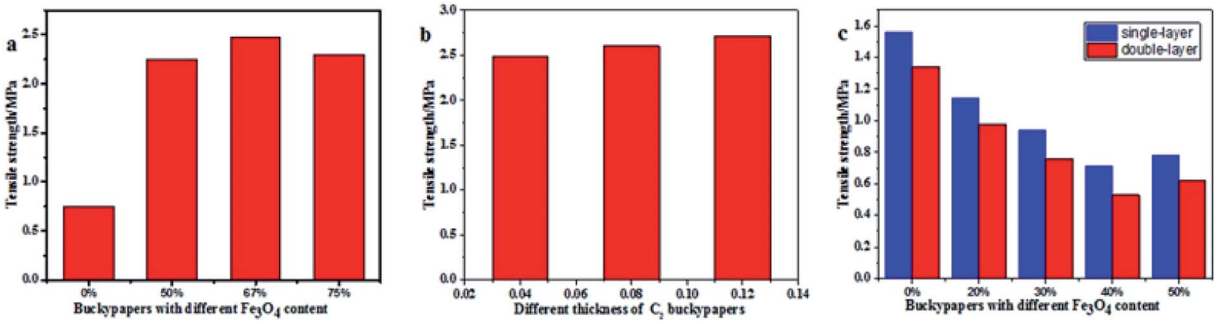

Fig. 8 Tensile strengths of Fe_3O_4/MWCNT buckypapers with (a) different Fe_3O_4 contents, (b) different thicknesses of C_2 buckypapers and (c) Fe_3O_4/GO buckypapers with different Fe_3O_4 contents.

of Fe_3O_4 to MWCNT increases, the electromagnetic absorption properties of Fe_3O_4/MWCNT hybrid buckypapers showed a tendency to first strengthen and subsequently weaken. The absorption bandwidth shows the same trend; this may be due to the increase in ion displacement and electric dipole polarisation as the iron content increases.

As the interfacial area of the Fe_3O_4-wrapped MWCNT structures increased, the electromagnetic wave absorption performance of the hybrid buckypapers improved. When the Fe_3O_4 content reached 75%, aggregation of the MWCNT significantly affected the dispersion state of the Fe_3O_4/MWCNT buckypapers, and weakened the electromagnetic wave-absorption properties. In all the samples, C_2 buckypaper showed the lowest absorption peak (−26.4 dB at 16.3 GHz) and the largest bandwidth, which represents a compromise between dielectric loss (dominant role) and magnetic loss.

Fig. 9b shows the RL values of C_2 buckypapers with different thicknesses, which indicates that the minimum RL is −14.4 dB

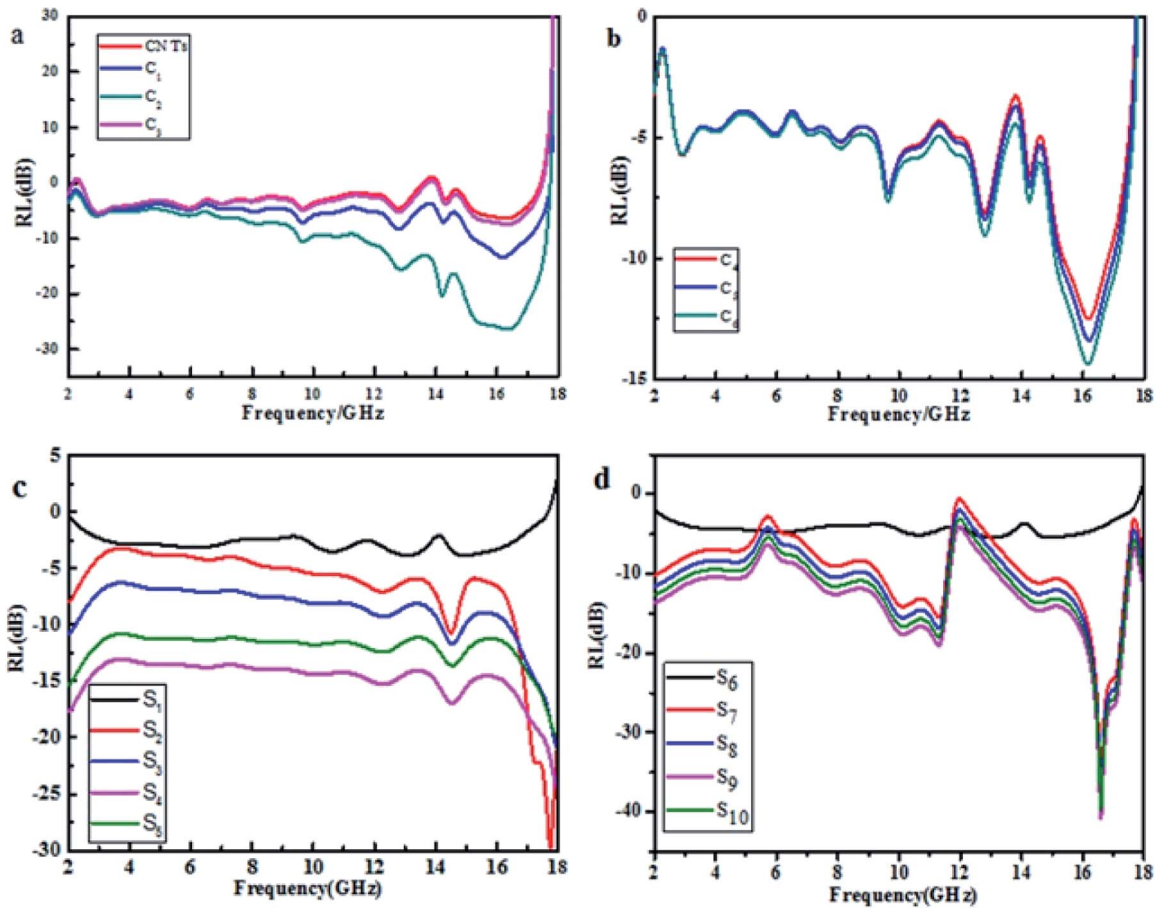

Fig. 9 Electromagnetic RL of Fe_3O_4/MWCNT buckypapers with different Fe_3O_4 contents (a) and different thicknesses of C_2 (b), single-layer (c) and double-layer (d) Fe_3O_4/GO buckypapers with different Fe_3O_4 contents (S_1, S_6: 0 wt%, S_2, S_7: 20 wt%, S_3, S_8: 30 wt%, S_4, S_9: 40 wt% and S_5, S_{10}: 50 wt%).

at 16.2 GHz and the bandwidth below −10 dB can reach 2.1 GHz (from 15.1 to 17.2 GHz) for a layer 0.12 mm thick. When the thickness of buckypaper is 0.04 mm, its minimum RL is −12.5 dB at 16.1 GHz, and the effective bandwidth below −10 dB is 1.5 GHz. The minimum RL increases to −13.4 dB at 16.2 GHz when the thickness of the hybrid buckypaper increases to 0.08 mm, and the bandwidth below −10 dB for this case can reach 1.8 GHz. Therefore, the thickness is one of the main factors affecting the absorption properties of buckypapers. The absorption intensity and effective absorption bandwidth of hybrid buckypapers increased as the thickness increased.

Fig. 9c shows the difference in electromagnetic RL with frequency between single-layer GO and Fe_3O_4/GO buckypapers. This shows that pure GO buckypaper exhibits poor microwave absorption performance compared with hybrid buckypapers, with its minimum RL reaching only −3.9 dB at 14.9 GHz. For the S_2 buckypaper, the minimum RL reaches −11.8 dB at 14.5 GHz and the RL bandwidth below −10 dB is 0.3 GHz (from 14.3 to 14.6 GHz). The minimum RL of S_3 buckypaper is −11.6 dB, and its RL bandwidth below −10 dB exceeds 0.7 GHz (from 14.2 to 14.9 GHz). For the S_5 buckypaper, the minimum RL reaches −13.6 dB at 14.5 GHz and the RL bandwidth below −10 dB spans the entire frequency range of 2.0–18.0 GHz. However, for S_4 buckypaper, the minimum RL can reach −17.0 dB at 14.5 GHz; further, this incorporates over 90% of the electromagnetic wave absorption over the entire frequency range. This phenomenon possibly occurs owing to the high GO contents in the S_2 and S_3 hybrid buckypapers leading to higher dielectric loss and poorer impedance, matching the performance of the Fe_3O_4/GO hybrid buckypapers. Regarding S_4 buckypaper, which has the most appropriate GO to Fe_3O_4 mass ratio of 6 : 4, it is essential to reduce the large dielectric constant to achieve impedance matching and enhance the microwave absorption by the hybrid buckypapers.

The RL values of double-layer GO and Fe_3O_4/GO buckypapers were tested in the range of 2.0–18.0 GHz, as shown in Fig. 9d. This shows that the thickness minimally affects the absorption properties of pure GO buckypaper, for which the minimum RL reaches only −5.5 dB at 14.9 GHz. The dependence curves of the RL on frequency for several Fe_3O_4/GO hybrid buckypapers are similar, the bandwidth is the main parameter affecting the absorption performance. The minimum RL of Fe_3O_4/GO hybrid buckypapers with different Fe_3O_4 contents can reach −35.3 dB at 16.6 GHz, −38.1 dB at 16.6 GHz, −41.0 dB at 16.5 GHz and −39.8 dB at 16.5 GHz. S_4 buckypaper has the minimum RL, which is consistent with the results shown in Fig. 9c.

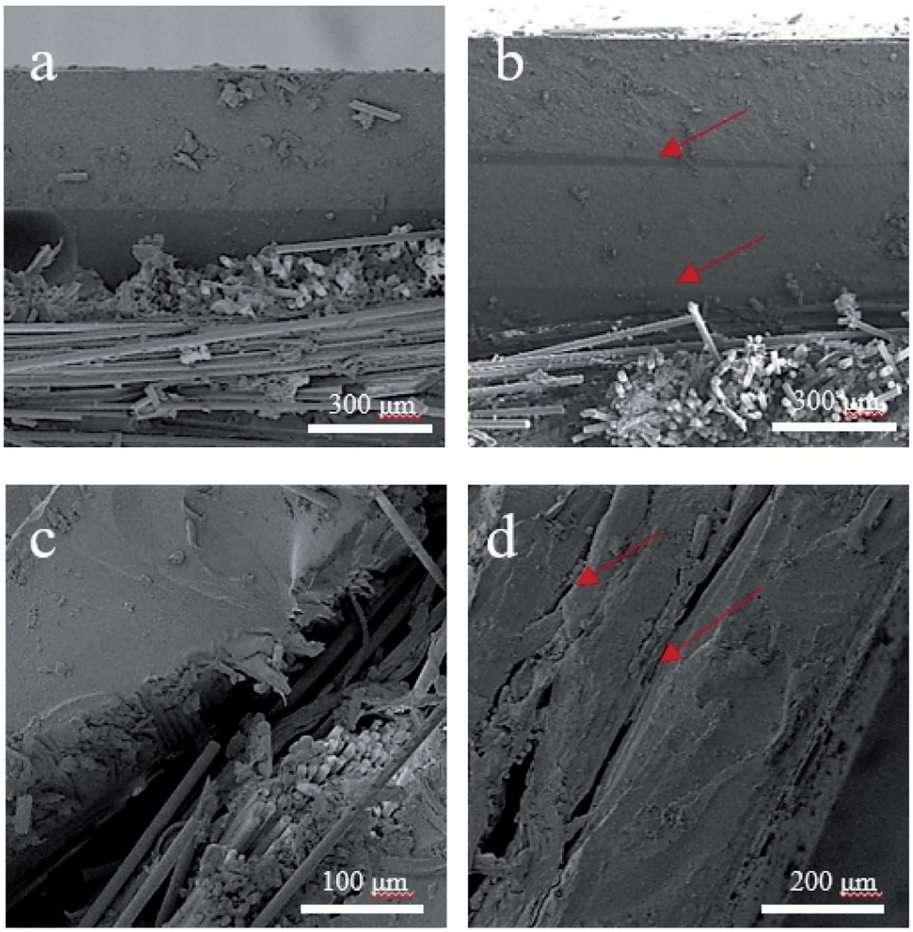

Fig. 10 SEM images of the fracture surfaces of Fe_3O_4/MWCNT buckypapers/EP/GF composites: (a) single-layer, (b) double-layer, and Fe_3O_4/GO buckypapers/EP/CF composites: (c) single-layer, (d) double-layer.

Table 1 Mechanical properties of composites

Sample	Flexural strength (MPa)	Flexural modulus (GPa)	Shear strength (MPa)	Tensile strength (MPa)
EP/GF	407.7(12.2[a])	2.9(0.3[a])	42.0(10.5[a])	188.3(14.6[a])
Single-layer Fe_3O_4/MWCNT/EP/GF	402.2(14.0[a])	2.7(0.5[a])	40.9(11.0[a])	185.8(12.4[a])
Double-layer Fe_3O_4/MWCNT/EP/GF	371.6(13.4[a])	2.5(0.2[a])	39.6(12.9[a])	182.7(13.4[a])
EP/CF	385.7(13.2[a])	5.8(0.5[a])	33.7(11.7[a])	318.6(13.6[a])
Single-layer Fe_3O_4/GO/EP/CF	370.6(14.5[a])	4.5(0.7[a])	28.1(11.4[a])	313.7(15.1[a])
Double-layer Fe_3O_4/GO/EP/CF	303.2(15.0[a])	4.1(0.3[a])	21.4(12.1[a])	315.0(11.6[a])

[a] Standard deviation of data.

A RL below −10 dB means that the material possesses 90% of the electromagnetic wave absorption, a RL below −20 dB means that the material possesses 99% of the electromagnetic wave absorption. It was found that as the content of Fe_3O_4 nanoparticles increased, the RL bandwidths below −10 dB for double-layer hybrid buckypapers were 3.3 GHz (from 14.0 to 17.3 GHz), 3.9 GHz (from 13.6 to 17.5 GHz), 4.4 GHz (from 13.1 to 17.5 GHz) and 4.1 GHz (from 13.4 to 17.5 GHz), showing a tendency to first increase and then decrease. Meanwhile, the RL bandwidths below −20 dB for hybrid buckypapers were 0.8 GHz (from 16.4 to 17.2 GHz), 0.9 GHz (from 16.3 to 17.2 GHz), 1.1 GHz (from 16.1 to 17.2 GHz) and 1.0 GHz (from 16.2 to 17.2 GHz).

The electromagnetic RL and absorption bandwidth are two significant factors that affect the absorption performance. The combination of dielectric GO and magnetic Fe_3O_4 in suitable proportions is the main reason for the improved wave-absorption performance. First, hybrid buckypapers can obtain better impedance matching, which is conducive to absorbing electromagnetic waves to the surface and thereby increasing attenuation. Second, the interface and dipole polarisation caused by the unique three-dimensional microstructure and multilayer structure of GO,[31] improve the absorption capacity of the hybrid buckypapers. To summarise, S_4 buckypaper can simultaneously obtain the minimum electromagnetic RL and maximum effective absorption bandwidth.

3.2 Structure and properties of composites

Fig. 10 shows the SEM images of the fracture surfaces of Fe_3O_4/MWCNT buckypapers/EP/GF and Fe_3O_4/GO buckypapers/EP/CF composites with different numbers of layers of buckypapers. Fig. 10a and b show the SEM images of the composites attached to single and double-layer of Fe_3O_4/MWCNT buckypapers, respectively. It is clear that there is no significant stratification, indicating good adhesion between Fe_3O_4/MWCNT buckypapers and the EP/GF composite matrix. An SEM image of Fe_3O_4/GO buckypapers/EP/CF composites coated with single-layer buckypapers is shown in Fig. 10c; the interface between the buckypaper and substrate has obvious lamination, demonstrating that the interface bonding is weak. Fig. 10d shows that the interface bonding performance between the double-layer buckypapers and substrate is poor; further, there is an obvious interface between the double-layer buckypapers, which is related to the loose-layered structure of GO.

The mechanical properties of various buckypapers/composites are summarised in Table 1. The change of tensile strength is not significant, but the flexural and shear strength of the composites deteriorated when attached to buckypapers compared with those of pure composites. The shear strength of the composites is influenced by the interfacial bonding strength between the buckypaper and matrix. Fe_3O_4/MWCNT buckypapers/EP/GF composites have higher shear strength than

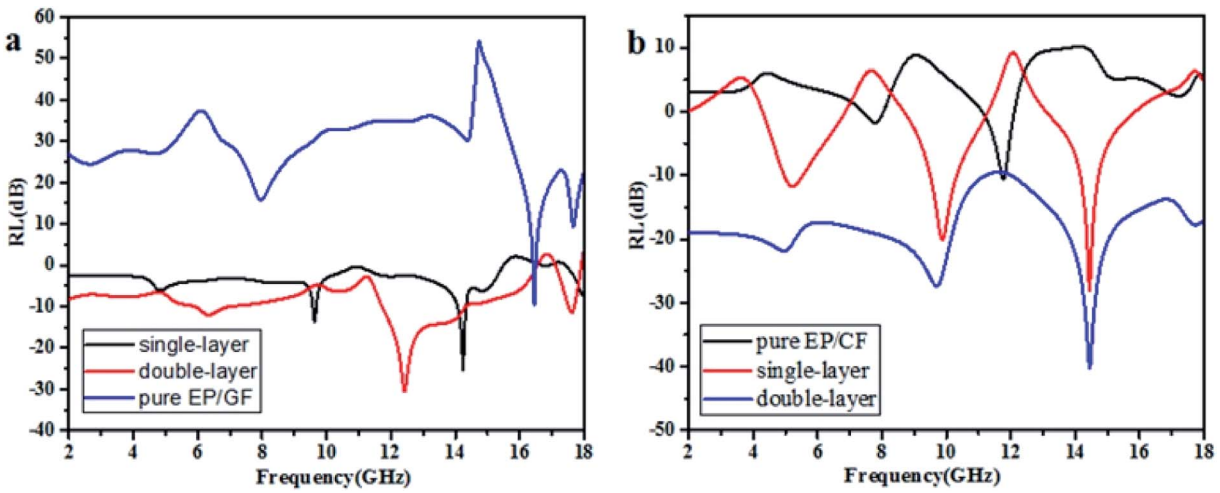

Fig. 11 Electromagnetic RL of Fe_3O_4/MWCNT buckypapers/EP/GF (a) and Fe_3O_4/GO buckypapers/EP/CF (b) composites with different numbers of layers of buckypapers.

Fe_3O_4/GO buckypapers/EP/CF composites, which is because GO buckypapers delaminate easily, resulting in a weakened interaction with the matrix. It is clear that composites coated with Fe_3O_4/MWCNT buckypapers have higher flexural strength than those coated with Fe_3O_4/GO buckypapers, this is attributed to the poor mechanical properties of the Fe_3O_4/GO buckypapers, which leads to weak parts in the composite and a significant decrease in bending strength. Besides, the mechanical properties of all the composites coated with two layers of buckypapers are poorer than those of the composites coated with one layer of buckypapers, which is due to the small bonding force between the buckypapers resulting in a low interfacial force and poor mechanical properties. This is consistent with the SEM images shown in Fig. 10.

The wave-absorption properties of Fe_3O_4/MWCNT buckypapers/EP/GF and Fe_3O_4/GO buckypapers/EP/CF composites with different numbers of layers of buckypapers are shown in Fig. 11. As shown in Fig. 11a, the pure EP/GF composite has an electromagnetic RL of −8.6 dB at 16.4 GHz. The minimum RL of Fe_3O_4/MWCNT buckypapers/EP/GF composites coated with single-layer buckypaper reached −25.8 dB at 14.2 GHz, and the RL bandwidth below −10 dB was 0.2 GHz (from 14.3 to 14.5 GHz). For Fe_3O_4/MWCNT buckypapers/EP/GF composites coated with double-layer buckypapers, a significant shift in the absorption band was observed compared with that of the former. The minimum RL can reach −31.2 dB at 12.4 GHz and the RL bandwidths below −10 and −20 dB were 2.5 and 0.4 GHz, respectively. The results show that the electromagnetic loss performance of Fe_3O_4/MWCNT buckypapers/EP/GF composites increases with the number of layers of buckypapers, presenting a significantly broadened effective absorption band. The displacement of the frequency band can be explained through the quarter wavelength principle, which is the relation between the thickness of the absorbing agent and frequency variation required to obtain the best absorption performance.[32,33] Here, if the thickness (t_m) must satisfy formula (1) at peak frequency (f_m):

$$t_m = nc/(4f_m(|\mu_r||\varepsilon_r|)^{1/2}),\ (n = 1, 3, 5, \ldots) \quad (1)$$

where $|\mu_r|$ and $|\varepsilon_r|$ are the moduli of μ_r and ε_r, and c is the speed of light. As the number of layers of externally attached buckypapers increases, *i.e.* the thickness of the absorbing layer increases, the double-layer buckypapers/EP/GF composite satisfies the relationship between t_m and f_m based on its attenuation-loss capability and moderate impedance matching properties. Thus, a better microwave-absorption performance is obtained at 12.4 GHz.

As shown in Fig. 11b, the pure EP/CF composite had a RL of −10.2 dB at 11.7 GHz and effective absorption band of 0.15 GHz below −10 dB. The RL of Fe_3O_4/GO buckypapers/EP/GF composites coated with single-layer buckypaper could reach −28.1 dB at 14.4 GHz, and the RL bandwidth below −10 dB was 2.1 GHz. The minimum RL value increased to −40.5 dB at 14.4 GHz when the EP/CF composite was pasted with double-layer buckypapers; its electromagnetic RL values were almost all below −10 dB from 2.0–18.0 GHz, and the RL bandwidth under −20 dB was 3.8 GHz. Generally, the minimum RL of buckypapers/EP/GF composites increased by 17.3 and 29.7 dB, and the effective absorption bands were broadened compared with those of the pure EP/CF composite.

Three absorption peaks appear for the Fe_3O_4/GO buckypapers/EP/CF absorbing composites owing to impedance matching. For multilayer absorbing materials, the surface resistance of the material and overall impedance must match the air impedance. During the matching process, two new impedances appear owing to the addition of the EP/CF composite substrate and interfacial polarisation is generated at the new interface, which improves the impedance matching and produces a strong absorption peak at the well-matched frequency.

An illustration of the principle of electromagnetic absorption by Fe_3O_4/GO hybrid buckypapers is shown in Fig. 12. A mismatch between the impedance of a single medium or magnetic composition and that of air always prevents the incoming electromagnetic wave from entering the adsorbent, resulting in low absorption efficiency. The layered interpenetrating structure of GO can generate multiple reflections, thus extending the propagation path of electromagnetic waves.

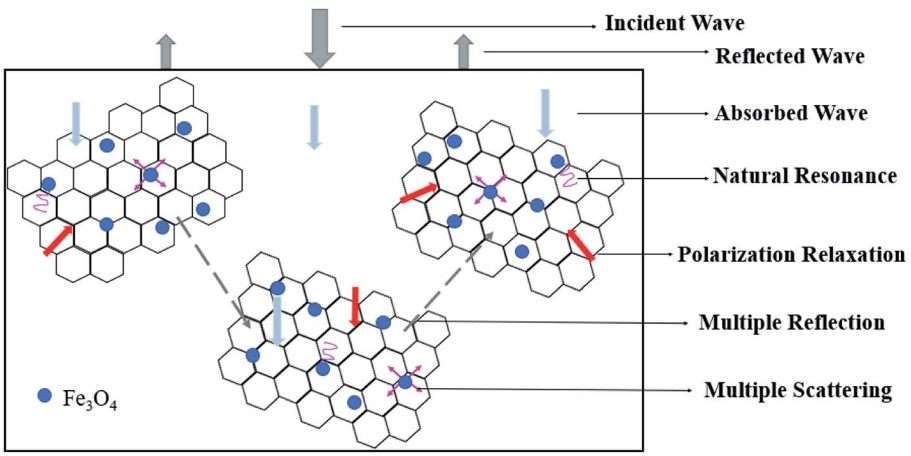

Fig. 12 Illustration of the principle of electromagnetic absorption by Fe_3O_4/GO hybrid buckypapers.

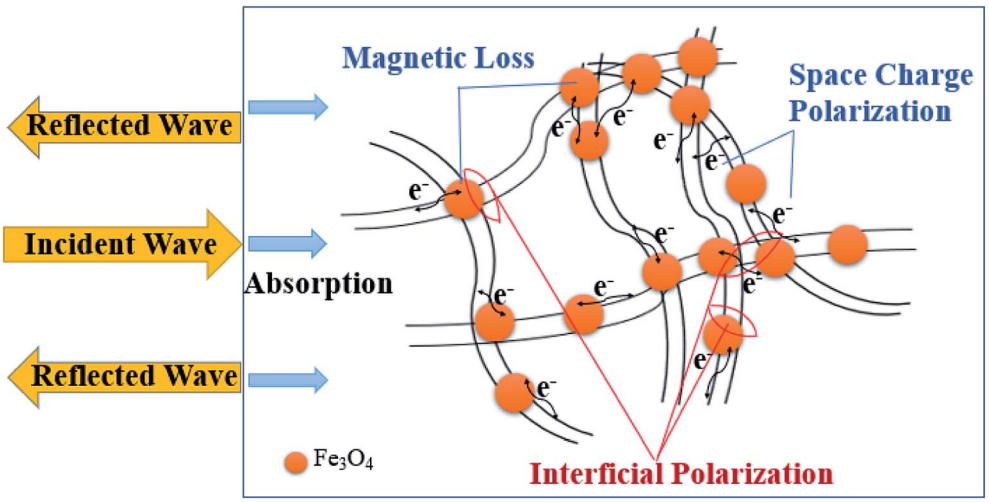

Fig. 13 Illustration of the principle of electromagnetic absorption by Fe_3O_4/MWCNT hybrid buckypapers.

The dipole polarisation is caused by the nanoparticles deposited on GO, for which the Fe_3O_4 nanoparticles are regarded as the polarisation centre. Additionally, introducing GO increases the boundary and surface anisotropy of nano-crystalline iron. The rotation and displacement of the Fe_3O_4 nanoparticle domain generate natural and exchange resonance.[34] Finally, the residual defects and groups on the GO sheet improve the polarisation relaxation and the absorption capacity of the hybrid buckypapers.

Fig. 13 illustrates the principle of electromagnetic absorption using Fe_3O_4/MWCNT hybrid buckypapers. The special helical structure and electromagnetic effects of one-dimensional carbon nanotubes lead to the dielectric relaxation of hybrid buckypapers, which contributes significantly to enhancing the electromagnetic microwave-absorption properties. The enhanced polarisation relaxation mainly originates from defects in the carbon nanotubes, which can be used as polarisation centres; further, the abundant oxygen functional groups and iron nanoparticles can produce hybrid atoms with different electronegativities, which contribute to the generation of the electron dipole polarisation.[2] Additionally, interfacial polarisation between Fe_3O_4 nanoparticles loaded on carbon nanotubes and the carbon nanotubes improves the absorbency of the Fe_3O_4/MWCNT hybrid buckypapers.

To summarise, the structural characteristics of carbon nanotubes and GO are markedly different, leading to a difference in the absorption properties of Fe_3O_4/MWCNT and Fe_3O_4/GO buckypapers.[35] First, the lamellar structure of GO is more conducive to nanoparticle adhesion, enhancing the interfacial polarisation between the nanoparticles and GO. Second, the lamellar interpenetrating structure provides more opportunities for multiple reflection and absorption of electromagnetic waves, so that the electromagnetic waves are ultimately effectively attenuated. Third, many residual groups in GO can effectively improve polarisation relaxation and enhance the microwave absorption properties.

4. Conclusion

Fe_3O_4/MWCNT and Fe_3O_4/GO hybrid buckypapers prepared *via* simple vacuum filtration and evaporation-induced self-assembly, respectively, have been successfully applied to epoxy resin/fibre substrates to fabricate absorbing composite materials. We demonstrated that owing to the structural differences in the buckypapers, Fe_3O_4/MWCNT buckypapers exhibit superior toughness and mechanical properties in comparison with Fe_3O_4/GO buckypapers and their coating on the substrate is better and much easier to operate. However, their microwave-absorption properties are inferior to those of Fe_3O_4/GO buckypapers, which is due to the effective complementarity of the dielectric and magnetic losses of the latter. Excellent absorption properties can be obtained by attaching these two hybrid buckypapers to the epoxy resin substrate, of which Fe_3O_4/GO buckypapers/EP/CF composites have better wave-absorption properties, and their mechanical properties are not significantly affected. Generally, Fe_3O_4/MWCNT and Fe_3O_4/GO buckypapers can be used as alternative microwave-absorbing coatings for preparing absorbing composites, and these are expected to meet the demand for lightweight microwave-absorbing composite materials.

Conflicts of interest

There are no conflicts to declare.

Acknowledgements

The authors gratefully acknowledge the financial support from the National Natural Science Foundation of China (No. 51373135) and the Seed Foundation of Innovation and Creation for Graduate Students (ZZ2019228) in Northwestern Polytechnical University, the Analytical & Testing centre of Northwestern Polytechnical University for the support of SEM, TEM and other instruments used in this paper.

References

1 C. Wang, X. J. Han, P. Xu, X. L. Zhang, Y. C. Du, S. R. Hu, J. Y. Wang and X. H. Wang, *Appl. Phys. Lett.*, 2011, **98**(7), 072906.
2 Y. C. Yin, M. Zeng, J. Liu, W. K. Tang, H. R. Dong and R. Z. Xia, *Sci. Rep.*, 2016, **6**, 25075.
3 H. Luo, R. Z. Gong, X. Wang, K. Song, C. M. Zhu and L. G. Wang, *New J. Chem.*, 2016, **40**(7), 6238–6243.
4 L. Y. Zhu, X. J. Zeng, M. Chen and R. H. Yu, *RSC Adv.*, 2017, **7**(43), 26801–26808.
5 Q. Zhou, K. H. Liu, X. M. Xiong, F. Wang and L. W. Lin, *Carbon*, 2012, **50**(3), 1179–1185.
6 T. George, T. Dimitrios, A. Christos, P. John, G. Costasa and P. Konstantinos, *Compos. Sci. Technol.*, 2013, **77**, 52–59.
7 T. N. Narayanan, Z. Liu, P. R. Lakshmy, W. Gao, N. Yutaka, D. S. Kumar, J. Lou, R. Vajtai and P. M. Ajayan, *Carbon*, 2012, **50**(3), 1338–1345.
8 S. W. Lu, W. K. Xu, X. H. Xiong, K. M. Ma and X. Q. Wang, *J. Alloys Compd.*, 2014, **606**, 171–176.
9 C. J. Yuan, *Preparation and wave absorption of carbon nanotube/ferrite hybrid films*, Shenyang Aerospace University, 2016.
10 M. F. Arif, S. Kumar and T. Shah, *Mater. Des.*, 2016, **101**, 236–244.
11 J. W. Zhang, D. Z. Jiang and H. X. Peng, *Microporous Mesoporous Mater.*, 2014, **184**, 127–133.
12 M. H. Rashid, S. Q. T. Pham, L. J. Sweetman, L. J. Alcock, A. Wise, L. D. Nghiem, G. Triani, M. I. H. Panhuis and S. F. Ralph, *J. Membr. Sci.*, 2014, **456**, 175–184.
13 Y. X. Xu, H. Bai, G. W. Lu, C. Li and G. Q. Shi, *J. Am. Chem. Soc.*, 2008, **130**, 5856–5857.
14 B. C. Mattevi, G. Eda, S. Agnoli, S. Miller, K. A. Mkhoyan and O. Celik, *Adv. Funct. Mater.*, 2009, **19**(16), 2577–2583.
15 E. Ou, X. J. Zhang, Z. M. Chen, Y. G. Zhan, Y. Du and G. P. Zhang, *Chemistry*, 2011, **17**(32), 8789–8793.
16 J. T. Robinson, M. Zalalutdinov, J. W. Baldwin, E. S. Snow, Z. Q. Wei and P. Sheehan, *Nano Lett.*, 2008, **8**(10), 3441–3445.
17 H. C. Schniepp, J. L. Li, M. J. McAllister, H. Sai, H. A. Margarita and D. H. Adamson, *J. Phys. Chem. B*, 2006, **110**(17), 8535–8539.
18 L. J. Cote, F. Kim and J. X. Huang, *J. Am. Chem. Soc.*, 2009, **131**(3), 1043–1049.
19 S. Gilje, S. Han, M. S. Wang, K. L. Wang and R. B. Kaner, *Nano Lett.*, 2007, **7**(11), 3394–3398.
20 X. Wang, L. J. Zhi and K. Mullen, *Nano Lett.*, 2008, **8**(1), 323–327.
21 J. L. Rigueur, S. A. Hasan, S. V. Mahajan and J. H. Dickerson, *Carbon*, 2010, **48**(14), 4090–4099.
22 M. M. MacInnes, S. Hlynchuk, S. Acharya, N. Lehnert and S. Maldonado, *ACS Appl. Mater. Interfaces*, 2018, **10**(2), 2004–2015.
23 D. A. Dikin, S. Stankovich, E. J. Zimney, R. D. Piner, G. H. Dommett, G. Evmenenko, S. T. Nguyen and R. S. Ruoff, *Nature*, 2007, **448**(7152), 457–460.
24 J. J. Liang, Y. F. Xu, D. Sui, L. Zhang, Y. Huang, Y. F. Ma, F. F. Li and Y. S. Chen, *J. Phys. Chem. C*, 2010, **114**, 17465–17471.
25 X. Jiang, R. J. Zhang, T. T. Yang, S. Y. Lin, Q. Chen, Z. Zhen, D. Xie and H. W. Zhu, *Surf. Coat. Technol.*, 2016, **299**, 22–28.
26 J. X. Wang, G. Wang and H. Wang, *Electrochim. Acta*, 2015, **182**, 192–201.
27 C. F. Xiao, Y. F. Tan, X. L. Wang, L. Gao, L. L. Wang and Z. H. Qi, *Chem. Phys. Lett.*, 2018, **703**, 8–16.
28 J. W. Li, J. J. Wei, Z. J. Pu, M. Z. Xu, K. Jia and X. B. Liu, *J. Magn. Magn. Mater.*, 2016, **399**, 81–87.
29 C. Q. Ma, *Microwave absorption and mechanical properties of carbon fiber reinforced graphene/Fe_3O_4 composite films*, Jilin University, 2017.
30 A. Mishra and T. Mohanty, *Integr. Ferroelectr.*, 2017, **184**(1), 178–185.
31 T. H. Wang, Y. F. Li, L. Wang, C. Liu, S. Geng, X. L. Jia, F. Yang, L. Y. Zhang, L. P. Liu, B. You, X. Ren and H. T. Yang, *RSC Adv.*, 2015, **5**, 60114–60120.
32 X. H. Liang, B. Quan, G. B. Ji, W. Liu, H. Q. Zhao and S. S. Dai, *ACS Sustainable Chem. Eng.*, 2017, **5**(11), 10570–10579.
33 Q. Hu, X. S. Qi, H. B. Cai, R. Xie, L. Long, Z. C. Bai, Y. Jiang, S. J. Qin, W. Zhong and Y. W. Du, *Sci. Rep.*, 2017, **7**, 11213.
34 Y. H. Hou, H. L. Yuan, H. Chen, J. H. Shen and L. C. Li, *Sci. China: Chem.*, 2017, **60**(6), 740–747.
35 X. Huang, X. Yan, L. Xia, P. Wang, Q. Wang, X. Zhang, B. Zhong, H. Zhao and G. Wen, *Scr. Mater.*, 2016, **120**, 107–111.